**Article:**

Fayon, A. K., Hansen, L. N., Piazolo, S. orcid.org/0000-0001-7723-8170 et al. (2 more authors) (Accepted: 2025) Dislocation motion enhances Pb mobility in experimentally deformed apatite. Geology. ISSN: 0091-7613 (In Press)

# Dislocation motion enhances Pb mobility in experimentally deformed apatite

**Annia K. Fayon[1], Lars N. Hansen[1], Sandra Piazolo[2], Amanda Dillman[1] and William O. Nachlas[3]**

[1]*Department of Earth and Environmental Sciences, University of Minnesota-Twin Cities, MN, 55455, USA*

[2]*School of Earth and Environment, University of Leeds, LS2 9JT, UK*

[3] *Department of Geoscience, University of Wisconsin-Madison, WI, 53706, USA*

## ABSTRACT

The distribution of Pb in minerals provides a key window into deciphering the timescales of geologic processes. However, the role of deformation-induced dislocations on Pb mobility and redistribution remains largely unconstrained. We conducted a series of experiments to constrain the processes controlling Pb mobility during deformation of apatite. Torsion experiments on single crystals of Durango apatite at 300 MPa confining pressure and 1100°C resulted in gradual lattice distortion and a network of subgrain boundaries in response to dislocation nucleation, movement, and recovery. Results from a static diffusion experiment at the same P-T conditions with a Pb source are consistent with known rates of volume diffusion. In contrast, torsion of an apatite single crystal coated in a Pb source revealed substantial mobility of Pb during deformation. This sample developed similar deformation-related microstructures, containing increased concentrations of Pb in and near subgrain boundaries. Our results demonstrate that during crystal-plastic deformation of apatite at these experimental conditions, Pb is transported orders of magnitude farther than predicted by published diffusivities, highlighting the importance of *active* crystal-plastic deformation in enhancing Pb mobility in apatite. We suggest that this enhanced mobility results from the capture and drag of Pb in Cottrell atmospheres associated with mobile dislocations during crystal-plastic deformation.

Our results have important implications for geothermochronological analyses relying on Pb concentrations in apatite, which will be affected by deformation below the Pb diffusion closure temperatures. Similar effects are likely to extend to other trace elements in accessory phases.

## INTRODUCTION

The distribution of Pb in apatite is commonly used to constrain the timing and rates of a breadth of geologic processes (e.g., Chew and Spikings, 2021), yet little is known about the mechanisms by which Pb is mobilized in deformed and/or deforming apatite. Understanding the mechanisms by which the distribution of Pb in deformed accessory phases is modified is crucial for interpreting geochronological and thermochronological data (e.g., Engi et al., 2017). Work on engineering materials has revealed that crystal defects may modify the spatial distribution of trace-elements (e.g., Cadel et al., 2003), and similar processes have been inferred to occur in accessory minerals. In geological samples, atom-probe tomography analyses demonstrate that trace elements may preferentially segregate to and accumulate along dislocations in zircon (Piazolo et al., 2016; Peterman et al., 2016) and rutile (Verberne et al., 2022). The presence and/or activity of dislocations has been shown to explain apparent age domains in apatite (Odlum et al., 2022), monazite (e.g., Erickson et al., 2015; Fougerouse et al., 2021a), titanite (Corvò et al., 2023) and zircon (Reddy et al., 2007; Moser et al., 2009; Timms et al., 2011; Piazolo et al., 2012, 2016). It has been hypothesized that dislocations may redistribute Pb and affect the distribution of apparent dates in a mineral by either acting as fast diffusion pathways or by dragging of trace elements (e.g. zircon: Piazolo et al., 2016; olivine: (Ando et al., 2001); apatite: Odlum et al., 2022, monazite: (Fougerouse et al., 2021b)a, b). In the first case, fast diffusion pathways remaining after deformation will continue enhancing Pb mobility. In the second case, Pb mobility will only be enhanced during deformation. Solute atoms are attracted to dislocations to reduce the overall energy of the system, forming Cottrell atmospheres. These atmospheres then move with the dislocations during plastic deformation (Supp). Determining the importance of either mechanism for redistributing Pb is fundamental to interpreting acquired ages. For example, if active dislocation movement is necessary for isotopic re-distribution, the apparent age could constrain the timing of deformation itself (e.g. Piazolo et al. 2012).

Here we present a set of deformation and diffusion experiments designed to specifically assess the influence of either pre-existing (static) or active (dynamic) dislocations on Pb mobility and therefore the apparent diffusivity of Pb in apatite. We choose apatite because it is widely used to constrain numerous geologic processes (Chew and Spikings, 2021) and can be easily deformed in the laboratory.

# EXPERIMENTAL DESIGN

We conducted three high-pressure (300 MPa), high-temperature (1100°C) experiments on single crystals of Durango apatite in a Paterson gas-medium apparatus (Paterson and Olgaard, 2000). Experimental conditions are presented in the Supplementary Material[1].

The null diffusion experiment was conducted to assess the mobility of Pb with no deformation at the same pressure and temperature as subsequent experiments. The undeformed crystal was coated in $PbZrO_3$ ( ~ 1mm thick) and jacketed in nickel. The sample assembly was held at high PT at hydrostatic conditions for 5 hours.

The static diffusion experiment assessed the mobility of Pb *after* deformation and involved two steps (Fig. 1A). First, we deformed the single crystal in torsion at high PT to produce a dislocation microstructure. The crystal was aligned such that the torsion axis was normal to the basal plane and jacketed as above. Second, the sample was quenched, unjacketed, coated in $PbZrO_3$, and rejacketed for a diffusion experiment identical to our null diffusion experiment.

The dynamic diffusion experiment assessed the mobility of Pb *during* deformation. This torsion experiment was carried out in the same manner as the previous one. However, the sample was coated with $PbZrO_3$ powder before being deformed (Fig. 1B).

Following experiments, all samples were cut, polished, and analyzed using electron probe microanalysis (EPMA) for backscatter electron (BSE) imaging and chemical characterization and electron backscatter diffraction (EBSD) for quantitative orientation analyses (Figs. S1- S3).

# OBSERVED DEFORMATION AND Pb MOBILITY

The static and dynamic deformation experiments result in distinctly different macroscopic behavior. Mechanical data from the experiments illustrate that the single crystal is significantly stronger if the Pb source is present *during* deformation (Fig. 1C). Furthermore, the apatite crystal in the static experiment exhibits relatively little compositional variation aside from lead zirconate polished into quench cracks (Fig. 1D), whereas the apatite crystal in the dynamic experiment exhibits compositionally distinct bands parallel to the basal plane and normal to the torsion axis, as revealed by elevated BSE signal (i.e., Pb-enrichment; Fig. 1E).

*Deformation experiments produced significant lattice distortion and subgrain development*

EBSD analyses of both deformation experiments reveal that dislocation activity occurred during deformation (Figs. 2A, B). Deformed samples develop continuous lattice curvature and a network of subgrain and grain boundaries (Figs. 2A, B). In the static case, high-angle boundaries are dominant (Fig. 2A), indicating that recovery occurred during the post-deformation diffusion anneal, whereas in the dynamic experiment the boundaries are primarily low-angle (Fig. 2B).

Disorientation axes associated with subgrain boundaries are primarily normal to <*c*>, which is consistent with boundaries being composed of edge dislocations gliding in <*a*> within the basal plane. This slip system has been inferred to be active in naturally deformed apatite (Odlum et al., 2022) and was optimally oriented to maximize the resolved shear stress during torsional deformation. In addition, the general orientation of the crystal (Fig. 2A and B, unit-cell diagrams), demonstrates that <*c*> is rotated relative to the starting position normal to the shear plane. This rotation can be produced by glide of dislocations with Burgers vectors parallel to the <*c*>, consistent with the disorientation axes and observations in natural apatite (Odlum et al., 2022). Away from the subgrains, lattice curvature of ~15° over 150 µm (Fig. S1) results in a geometrically necessary dislocation density of ~$10^{13}$ $m^{-2,}$, assuming a Burgers vector of 1 nm for <*a*>.

*Pb mobility is only enhanced* during *crystal plastic deformation*

A critical relationship is apparent in the dynamic experiment between the bands of subgrains and the bands of Pb enrichment, which is lacking in the static experiment. High-resolution BSE imaging of the static experiment confirms the absence of detectable Pb along subgrain bands (Fig. 2C), and EPMA confirms no measurable Pb within its crystal lattice or subgrain boundaries (Fig. 2E, S2). In contrast, the dynamic diffusion experiment exhibits a demonstrably higher BSE signal (Fig. 2D) collocated with subgrain bands (Fig. 2B). EPMA analysis reveals that this elevated BSE signal corresponds to elevated Pb concentrations (Fig. 2F). These elevated Pb concentrations are not associated with decompression (quench) cracks formed at the end of the experiment (cf. Fig. 1E) or contamination from the Pb source during polishing (cf. Fig. 1D). Additional EPMA maps reveal that these Pb concentrations are associated with Ca depletion (Figs. S2). In summary, Pb is transported 200 to 500 µm into the sample interior through the apatite lattice along bands of substructure development *if and only if* deformation is ongoing.

# DISCUSSION AND CONCLUSIONS

## *Dislocation motion is necessary to increase apparent Pb diffusivity in apatite*

Our experiments document that Pb mobility in apatite is enhanced *during* crystal-plastic deformation. As evidenced by both the null and static experiments, in which no Pb infiltration is observed, static dislocations, subgrain boundaries, and grain boundaries do not produce a measurable increase in Pb mobility beyond simple lattice diffusion (Fig 2). This observation is consistent with lattice diffusion estimates based on known diffusivities of Pb in apatite ($3.6\times10^{-13}$ $cm^2/s$; (Cherniak et al., 1991), which predict a characteristic lattice diffusion length at our experimental conditions of ~1 µm. Alternatively, fast-path diffusion along dislocations could be as much as 3 to 4 orders of magnitude faster (e.g., Hirth and Kohlstedt, 2015). However, even with a pipe diffusivity of $3.6\times10^{-9}$ $cm^2/s$, the apparent bulk diffusivity is expected to increase by only ~30% (assuming distributed dislocations, a dislocation core radius of twice the Burgers vector magnitude, and a dislocation density of $10^{13}$ $m^{-2}$). In the most extreme case of only looking at diffusion *within* the subgrain boundaries, the characteristic diffusion length is still only 10s of µm (assuming the boundaries have a similar diffusivity to pipe diffusion and a dislocation density of $10^{14}$ $m^{-2}$, corresponding to a misorientation of ~10°). In summary, neither lattice nor fast-path diffusion of Pb can explain the apparent 100–500 µm of Pb transport observed in the dynamic experiment.

Alternatively, we argue that Pb is captured in and around dislocation cores in Cottrell atmospheres (Supp) and is dragged into the sample interior by mobile dislocations. This segregation and dragging is a well-known phenomenon in metals (e.g., Cottrell and Bilby, 1949; Blavette et al., 1999; Cadel et al., 2003), and importantly, the dragging of Cottrell atmospheres by dislocations may result in macroscopic hardening of the material (Takeuchi and Argon, 1976). Segregation is evidenced in our experiments by high Pb concentrations in regions of high dislocation density. Dragging is evidenced in our experiments by increased shear strength in the dynamic experiment relative to the static experiment (Fig. 1C). Segregation of trace elements to Cottrell atmospheres has also been observed in some natural settings, including in zircon (Piazolo et al., 2016), rutile (Verberne et al., 2022), monazite (Fougerouse et al., 2021), and xenotime (Joseph et al., 2024).

Our interpretation that enhanced Pb mobility in our dynamic experiment results from dislocation related Pb capture and dragging requires that dislocations move from the exterior to the interior of the sample in these experiments. This requirement is consistent with the inferred primary active slip system (slip on the basal plane in <*a*>) in combination with the geometry of torsional deformation (Fig. 3A). We suggest that dislocation loops nucleate at the outer edge of the sample where stresses and strain rates are highest, and as the loops expand, the captured Pb is dragged inwards from the sample exterior (Fig. 3B). None of the Zr, which was also contained in the Pb source, is observed in the grain interior (Fig. S3) suggesting a preferential capture of Pb. The correlation between high Pb and low Ca concentrations in EPMA maps suggests that Pb is substituting for Ca in the lattice (Fig. S2). Furthermore, we argue Pb continues to concentrate along subgrain boundaries as dislocations organize during syn-deformation recovery (Figs. 2, 3B-D).

## *Implications for U-Pb dates in deformed apatite*

The experiments presented here were conducted in the absence of fluids and demonstrate that dislocations can drag Pb, in what we interpret to be Cottrell atmospheres, through an apatite crystal during deformation. This process produces heterogenous Pb distributions within a deforming grain as dislocations migrate, accumulate, and arrange into subgrain boundaries, resulting in apparent orders of magnitude faster transport than other diffusion mechanisms. In our experiments, the torsional geometry dictates that dislocations primarily move from the edge of the sample inwards. However, in nature, we envision that Pb primarily migrates with dislocations toward grain boundaries, effectively removing Pb from the grain. The enhanced mobility of Pb during deformation can skew thermochronometric dates obtained from U-Pb dating of apatite and potentially other accessory minerals that record crystal-plastic deformation (Piazolo et al., 2012; Moser et al., 2022). It is important to note that apatite can record crystal-plastic deformation below the closure temperature for Pb.

To assess the impact of our results on the interpretation of thermochronometric data, we consider the effect of timing of deformation on apatite grains in the absence of fluids after they have cooled below the closure temperature ($T_c$) for Pb. During crystal-plastic deformation, mobile dislocations will work to remove Pb from the crystal interiors, potentially in a heterogeneous manner that removes more Pb in some regions than others. This heterogeneous Pb mobilization will produce regions of apparently younger dates. If deformation occurs soon after the grain has cooled below Tc then the subsequent accumulation of radiogenic Pb over time will obscure the age domains. If, however, deformation occurs after a significant amount of radiogenic Pb has accumulated, the heterogeneity of age domains will be greater and more observable. The younger age domains would be related to the timing of deformation. This scenario is similar to what has been observed in natural apatite (Odlum et al. 2022) and titanite (Moser et al. 2022; Corvo et al., 2023; Langone et al. 2025).

Here we highlight the implications of increased Pb mobility from the presence and activation of dislocations in apatite. Atom-probe tomography on other naturally deformed accessory phases has documented the increased concentration of other trace elements in these defects (Peterman et al., 2016; Verberne et al., 2022). Higher observed concentrations are consistent with movement of trace elements towards dislocations, consistent with fast-path diffusion and document the importance of this mechanism over geologic timescales. Here we show that another important mechanism, drag by dislocations *during* deformation, can significantly alter the distribution of a trace element in a deformed accessory phase, highlighting the need to assess the presence and nature of the deformation of the studied grains. Although we explicitly use apatite and U-Pb in these experiments, this process could be relevant to any mineral that experiences deformation enhanced mobility of trace elements and/or a daughter element.

## ACKNOWLEDGEMENTS

Thoughtful reviews by A. Ault, M. Odlum, D. Fougerouse and D. Chew greatly improved this contribution. We also acknowledge insightful discussion about this work with D. Kohlstedt, M. Zimmerman, J. Mitchell, and H. Wiesman. Fayon was supported by NSF-EAR award 1727203. Parts of this work were carried out in the Characterization Facility, University of Minnesota, which receives partial support from the NSF through the MRSEC (Award Number DMR-2011401) and the NNCI (Award Number ECCS-2025124) programs. SP and LH acknowledge the Cheney Fellowship (2021-2025) awarded to LH.

# FIGURE CAPTIONS

*Figure 1:* A and B) Schematic of sample assemblies. dashed box in A and B indicate location of D and E. C) Mechanical data for both deformation experiments. D and E) Sample-scale BSE images of both deformation experiments cut perpendicular to the basal plane. White dashed box in E indicate locations of Figure 2B, D, and F.

*Figure 2:* A and B) EBSD maps of substructure in static and dynamic diffusion experiments. Maps are colored by disorientation to a reference point, for which the orientation is shown by unit-cell diagrams. Grain boundaries (disorientations >10°) and subgrain boundaries (disorientations of 2-10°) indicated by black and gray lines, respectively. C and D) BSE images of regions in A and B. White dashed box indicates location of map in B. E and F) Qualitative EMP maps of Pb concentration in the same regions as C and D.

*Figure 3.* A) Schematic representation of slip in the apatite sample. Pb is drawn into the crystal by dislocation loops expanding into the sample interior. B-D) Progression of Pb entrained by dislocations at the edge of the sample. With increasing strain, dislocations organize into subgrain boundaries resulting in higher concentrations of Pb along those boundaries.

# REFERENCES

Ando, J., Shibata, Y., Okajima, Y., Kanagawa, K., Furusho, M., and Tomioka, N., 2001, Striped iron zoning of olivine induced by dislocation creep in deformed peridotites: Nature, v. 414, p. 893–895.

Blavette, D., Cadel, E., Fraczkiewicz, A., and Menand, A., 1999, Three-dimensional atomic-scale imaging of impurity segregation to line defects: Science, v. 286, p. 2317–2319.

Cadel, E., Fraczkiewicz, A., and Blavette, D., 2003, Atomic Scale Investigation of Impurity Segregation to Crystal Defects: Annual review of materials research, v. 33, p. 215–231.

Cherniak, D.J., Lanford, W.A., and Ryerson, F.J., 1991, Lead diffusion in apatite and zircon using ion implantation and Rutherford Backscattering techniques: Geochimica et cosmochimica acta, v. 55, p. 1663–1673.

Chew, D.M., and Spikings, R.A., 2021, Apatite U-Pb thermochronology: A review: Minerals (Basel, Switzerland), v. 11, p. 1095.

Corvò, S., Maino, M., Piazolo, S., Kylander-Clark, A.R.C., Orlando, A., Seno, S., and Langone, A., 2023, Crystal plasticity and fluid availability govern the ability of titanite to record the age of deformation: Earth and planetary science letters, v. 620, p. 118349.

Cottrell, A.H., and Bilby, B.A., 1949, Dislocation Theory of Yielding and Strain Ageing of Iron: Proceedings of the Physical Society. Section A, v. 62, p. 49.

Engi, M., Lanari, P., and Kohn, M.J., 2017, 1. Significant ages - an introduction to petrochronology, *in* Kohn, M.J., Engi, M., and Lanari, P. eds., Petrochronology, Berlin, Boston, De Gruyter, p. 1–12.

Erickson, T.M., Pearce, M.A., Taylor, R.J.M., Timms, N.E., Clark, C., Reddy, S.M., and Buick, I.S., 2015, Deformed monazite yields high-temperature tectonic ages: Geology, v. 43, p. 383–386.

Fougerouse, D., Cavosie, A.J., Erickson, T., Reddy, S.M., Cox, M.A., Saxey, D.W., Rickard, W.D.A., and Wingate, M.T.D., 2021a, A new method for dating impact events – Thermal dependency on nanoscale Pb mobility in monazite shock twins: Geochimica et cosmochimica acta, v. 314, p. 381–396.

Fougerouse, D., Reddy, S.M., Seydoux-Guillaume, A.-M., Kirkland, C.L., Erickson, T.M., Saxey, D.W., Rickard, W.D.A., Jacob, D., Leroux, H., and Clark, C., 2021b, Mechanical twinning of monazite expels radiogenic lead: Geology, v. 49, p. 417–421.

Hirth, G., and Kohlstedt, D.L., 2015, The stress dependence of olivine creep rate: Implications for extrapolation of lab data and interpretation of recrystallized grain size: Earth and planetary science letters, v. 418, p. 20–26.

Joseph, C., Fougerouse, D., Cavosie, A.J., Olierook, H.K.H., Reddy, S.M., Tacchetto, T., Quintero, R.R., Kennedy, A., Saxey, D.W., and Rickard, W.D.A., 2024, Towards a new impact geochronometer: Deformation microstructures and U-Pb systematics of shocked xenotime: Geochimica et cosmochimica acta, v. 374, p. 33–50.

Langone, A., Simonetti, M., Corvò, S., Bonazzi, M., Maino, M., Orlando, A., Braschi, E. and Piazolo, S., 2025. Reactive and resilient: the contrasting behaviour of monazite and titanite during deformation (the Forno-Rosarolo shear zone; Ivrea-Verbano Zone): Geological Magazine, 162, p.e18.

Moser, D.E., Davis, W.J., Reddy, S.M., Flemming, R.L., and Hart, R.J., 2009, Zircon U–Pb strain chronometry reveals deep impact-triggered flow: Earth and planetary science letters, v. 277, p. 73–79.

Moser, A.C., Hacker, B.R., Gehrels, G.E., Seward, G.G.E., Kylander-Clark, A.R.C., and Garber, J.M., 2022, Linking titanite U–Pb dates to coupled deformation and dissolution–reprecipitation: Contributions to mineralogy and petrology. Beitrage zur Mineralogie und Petrologie, v. 177, doi:10.1007/s00410-022-01906-9.

Odlum, M.L., Levy, D.A., Stockli, D.F., Stockli, L.D., and DesOrmeau, J.W., 2022, Deformation and metasomatism recorded by single-grain apatite petrochronology: Geology, v. 50, p. 697–703.

Paterson, M.S., and Olgaard, D.L., 2000, Rock deformation tests to large shear strains in torsion: Journal of Structural Geology, v. 22, p. 1341–1358.

Peterman, E.M., Reddy, S.M., Saxey, D.W., Snoeyenbos, D.R., Rickard, W.D.A., Fougerouse, D., and Kylander-Clark, A.R.C., 2016, Nanogeochronology of discordant zircon measured by atom probe microscopy of Pb-enriched dislocation loops: Science advances, v. 2, p. e1601318.

Piazolo, S., Austrheim, H., and Whitehouse, M., 2012, Brittle-ductile microfabrics in naturally deformed zircon: Deformation mechanisms and consequences for U-Pb dating: The American mineralogist, v. 97, p. 1544–1563.

Piazolo, S., La Fontaine, A., Trimby, P., Harley, S., Yang, L., Armstrong, R., and Cairney, J.M., 2016, Deformation-induced trace element redistribution in zircon revealed using atom probe tomography: Nature communications, v. 7, p. 10490.

Reddy, S.M., Timms, N.E., Pantleon, W., and Trimby, P., 2007, Quantitative characterization of plastic deformation of zircon and geological implications: Contributions to mineralogy and petrology. Beitrage zur Mineralogie und Petrologie, v. 153, p. 625–645.

Takeuchi, S., and Argon, A., 1976, Steady-state creep of alloys due to viscous motion of dislocations☆: Acta Metallurgica, v. 24, p. 883–889.

Timms, N.E., Kinny, P.D., Reddy, S.M., Evans, K., Clark, C., and Healy, D., 2011, Relationship among titanium, rare earth elements, U–Pb ages and deformation microstructures in zircon: Implications for Ti-in-zircon thermometry: Chemical geology, v. 280, p. 33–46.

Verberne, R., Reddy, S.M., Saxey, D.W., Fougerouse, D., Rickard, W.D.A., Quadir, Z., Evans, N.J., and Clark, C., 2022, Dislocations in minerals: Fast-diffusion pathways or trace-element traps? Earth and planetary science letters, v. 584, p. 117517.

[1] Supplemental Material. [Details of deformation experiments, scanning electron microscopy, and electron microprobe analyses] Please visit https://doi.org/10.1130/XXXX to access the supplemental material, and contact editing@geosociety.org with any questions.

291 Figure 1

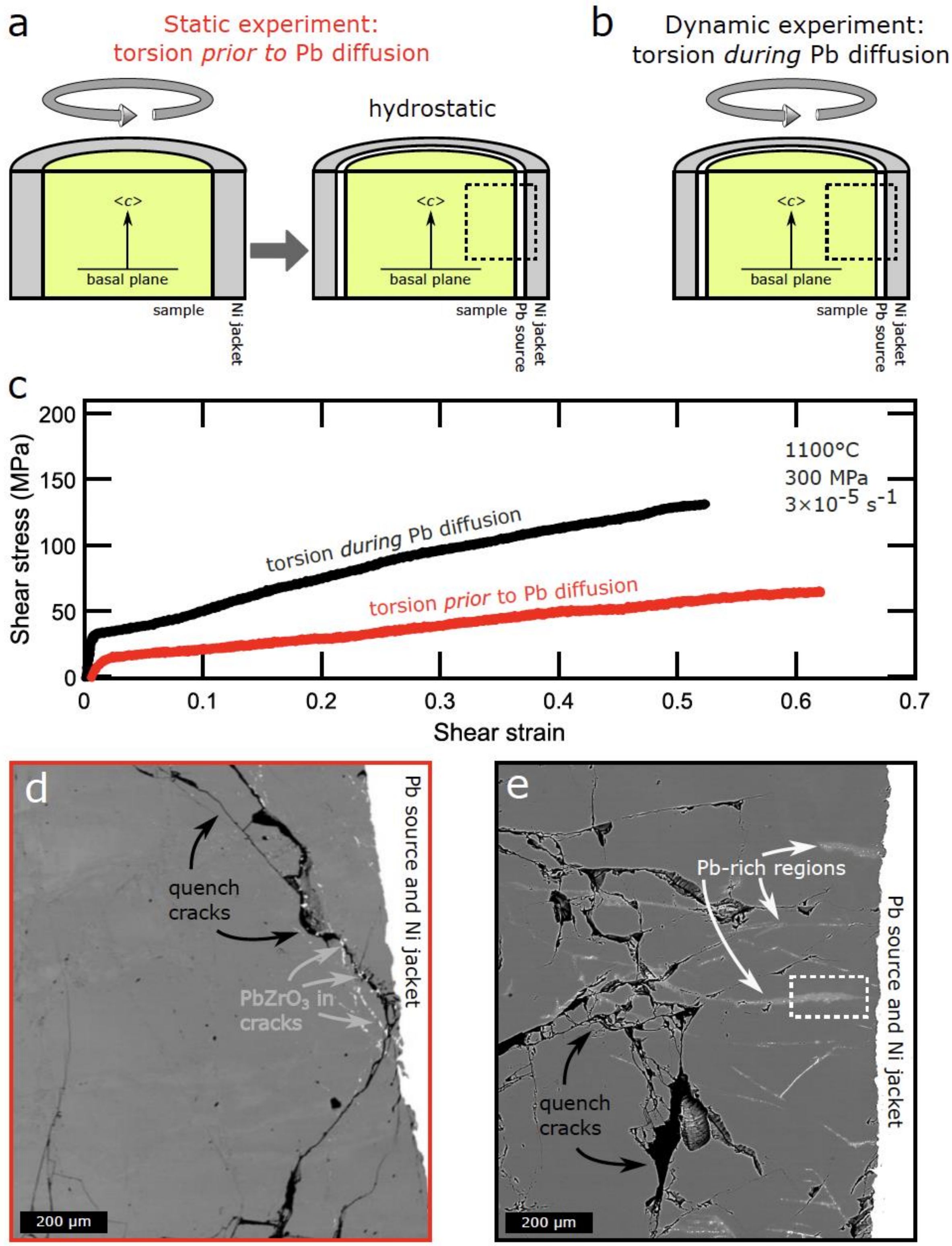

292

293

294

Figure 2

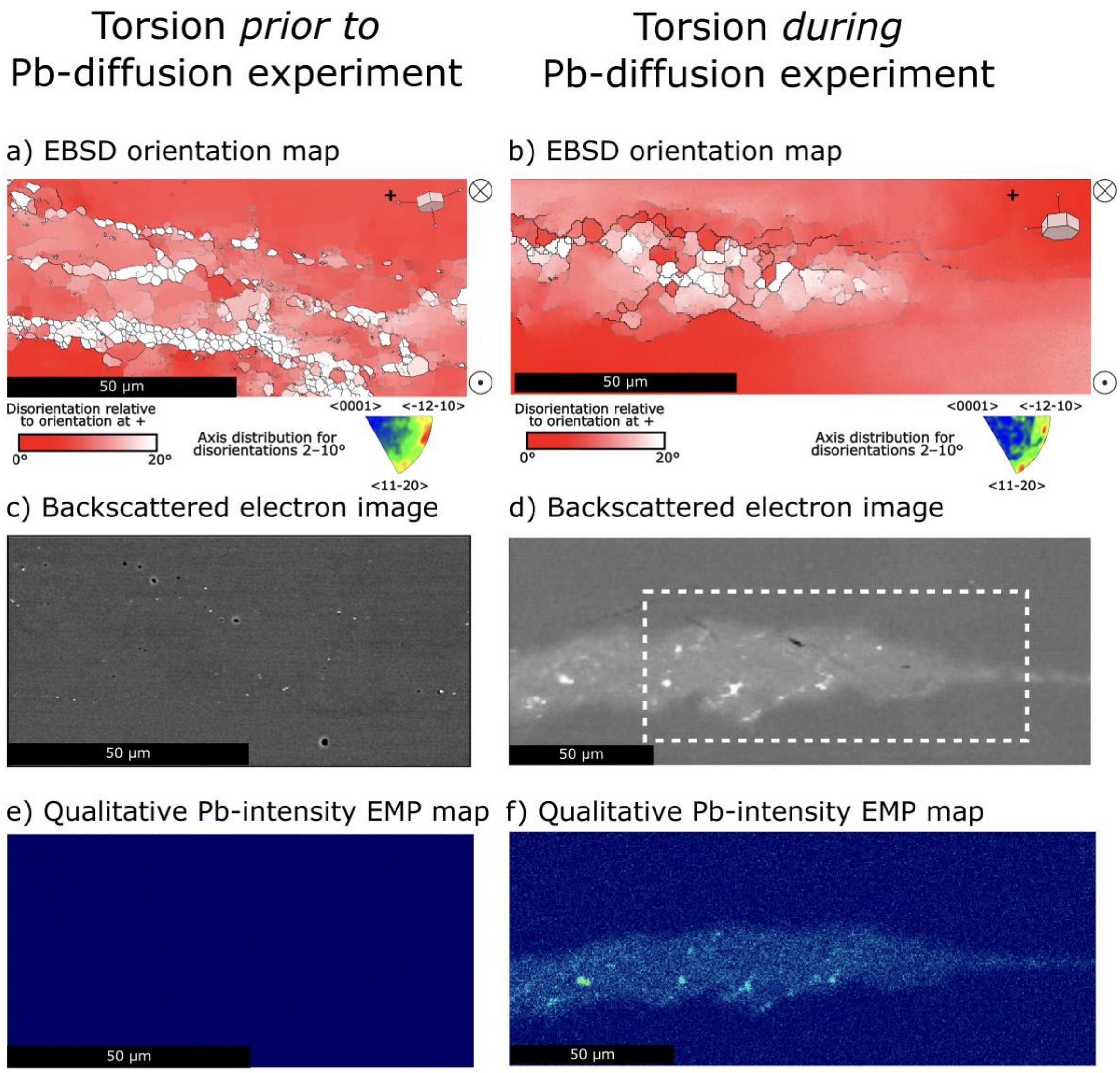
Torsion *prior to*
Pb-diffusion experiment
Torsion *during*
Pb-diffusion experiment
a) EBSD orientation map
b) EBSD orientation map
+
50 µm
Disorientation relative to orientation at +
0°
20°
Axis distribution for disorientations 2–10°
<0001>
<-12-10>
<11-20>
c) Backscattered electron image
d) Backscattered electron image
50 µm
e) Qualitative Pb-intensity EMP map
f) Qualitative Pb-intensity EMP map
50 µm

Figure 3

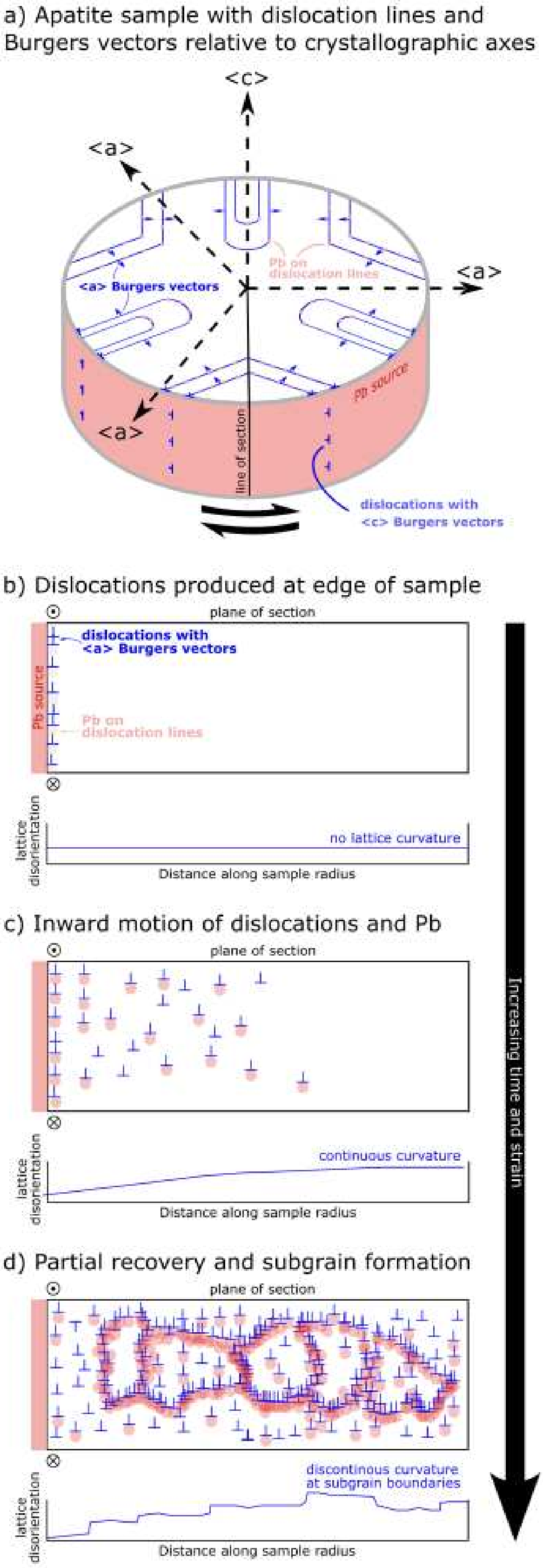
a) Apatite sample with dislocation lines and Burgers vectors relative to crystallographic axes
<c>
<a>
<a>
<a>
<a> Burgers vectors
Pb on dislocation lines
Pb source
line of section
dislocations with <c> Burgers vectors
b) Dislocations produced at edge of sample
plane of section
dislocations with <a> Burgers vectors
Pb source
Pb on dislocation lines
lattice disorientation
no lattice curvature
Distance along sample radius
c) Inward motion of dislocations and Pb
plane of section
lattice disorientation
continuous curvature
Distance along sample radius
d) Partial recovery and subgrain formation
plane of section
lattice disorientation
discontinous curvature at subgrain boundaries
Distance along sample radius
Increasing time and strain

# SUPPLEMENTAL MATERIALS

*Section A: A brief note on Cottrell Atmospheres*

Segregation and dragging of impurities by dislocations is a well-known phenomenon in metals and ceramics (e.g., Cottrell and Bilby, 1949; Blavette et al., 1999; Cadel et al., 2003). Distortion of the crystal lattice around a dislocation results in local lattice sites that are more energetically favorable for impurity atoms than pristine lattice. This energetic benefit drives segregation of impurities from the surrounding area to the distorted areas near dislocations. The regions around dislocations into which impurities are segregated are referred to as Cottrell atmospheres (Cottrell and Bilby, 1949). In theory, these atmospheres can form at any temperature due to the driving force from the presence of dislocations, and the rate at which they form is dependent on a number of variables including temperature, stress, strain rate, and dislocation density. The rate of segregation of the impurities is controlled by their lattice diffusivity. At higher temperatures, the lattice diffusivity is higher, which will in turn enhance the rate at which the atmosphere forms. Once the atmosphere forms around a dislocation, it will move through the crystal with the defect. A Cottrell atmosphere around a dislocation results in a hardening or strengthening of the material, as it becomes more difficult for the dislocation to move through the lattice with the atmosphere in tow (c.f Fig. 1C). If the applied stress is high enough, a dislocation can break free of the Cottrell atmosphere, leaving a region with higher concentrations of impurities.

*Section B: High-temperature, high-pressure deformation experiments*

Apatite single crystals were cut into wafers approximately 3 mm thick ranging between 7 and 9 mm in diameter. Wafers were orientated with <*c*> parallel to the cylindrical axis of the sample. In each experiment, apatite samples were placed between porous alumina spacers and first jacketed in Ni and then in Fe. In some experiments, the sample was initially coated with $PbZrO_3$ powder around the outer circumference prior to being jacketed. The $PbZrO_3$ compound was chosen as a Pb source due to its refractory nature.

Completed sample assemblies were then inserted into a Paterson gas-medium apparatus (Paterson and Olgaard, 2000). The vessel was pressurized to 300 MPa using argon as the pressure medium, and the sample was heated to 1100°C with a furnace internal to the pressure vessel. For each experiment, the sample was held at the target conditions for 5 hours.

In our null experiment, the crystal was coated in $PbZrO_3$ and then brought to target conditions with no deformation applied at any stage. In our static-diffusion experiment, the crystal was brought to target conditions and then deformed in torsion for 5 hours. The sample was quenched, removed from the assembly, coated with $PbZrO_3$, rejacketed, and brought back to target conditions for an additional 5 hours with no further deformation. In our dynamic-diffusion experiment, the crystal was initially coated in $PbZrO_3$, brought to target conditions, and then deformed in torsion for 5 hours.

In experiments involving torsional deformation, a constant twist rate was applied. This twist rate was set based on the sample dimensions such that the shear strain rate at the outer radius was $3\times10^{-5}$ $s^{-1}$. The torque necessary to maintain that rate was recorded throughout the experiment. Torque data were corrected for the strength of the jacket material using published flow laws for Ni and Fe (Frost and Ashby, 1982). Torque data were then converted to shear stress at the outer radius following the procedure outlined by Paterson and Olgaard (2000) with a stress exponent of 2, which has been previously measured in compression experiments on single crystals of apatite (Fayon and Hansen, 2018). Shear stresses throughout each deformation experiment are presented in Fig. 1c. Both experiments exhibited significant strain hardening. There is a notable increase in strength for the sample coated in $PbZrO_3$ before deformation.

### *Section C: Electron backscatter diffraction analysis (EBSD)*

Longitudinal sections of the deformed apatite crystals were cut and polished with diamond suspensions of decreasing size down to 0.05 µm. Samples were subsequently analyzed in a Thermo Apreo 2S Lo-Vac scanning electron microscope in the Characterization Facility at the University of Minnesota. Data were acquired using a beam current of 26 nA, an accelerating voltage of 20 kV, a working distance of 15 mm, and a stage tilt of 70°. An Oxford Instruments Symmetry detector for electron backscatter diffraction was used to collect maps of crystal orientation with a 0.2 µm step size.

Subsequent to mapping, EBSD data were processed using the Oxford Instruments AZtec Crystal software package. The processing routine consisted of removing wild spikes, interpolating orientations for missing pixels based on five nearest neighbors, and finally correcting for systematic misindexing of apatite by 60° around <*c*>. In construction of maps and inverse pole figures, grain boundaries were defined as misorientations between neighboring pixels of >10° and subgrain boundaries were defined as misorientations of 2 to 10°. Data used to calculate geometrically necessary dislocation density using equation 13 from REF are shown in Fig. S1.

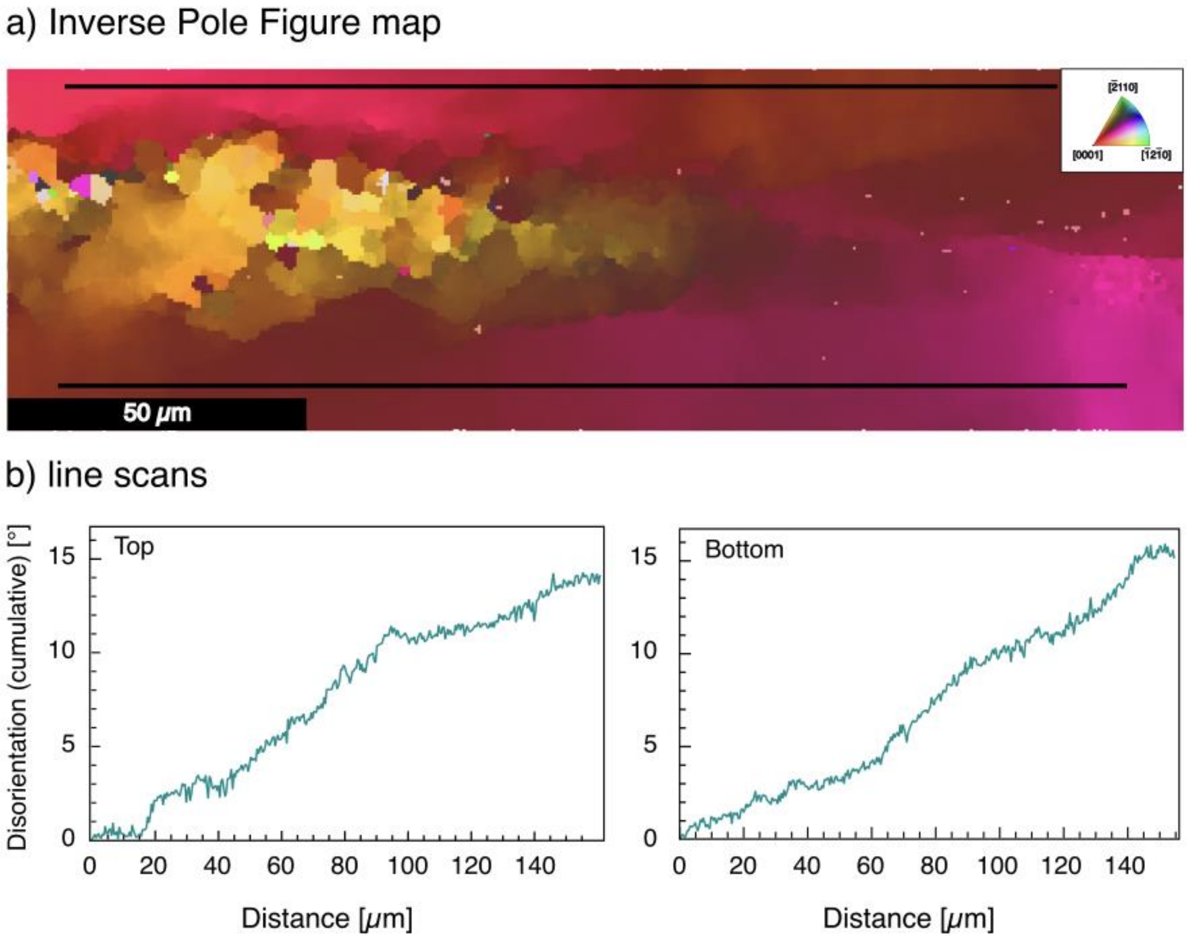

Figure S1. Radial transects across dynamic deformation experiment. A. Inverse pole figure map is shown relative to the vertical axis. Black lines indicate locations of line scans shown in B. Data document a lattice curvature of ~15° over ~150 µm, corresponding to a geometrically necessary dislocation density of ~$10^{13}$ $m^{-2}$.

### *Electron microprobe analysis (EPMA)*

Backscatter electron (BSE) images and qualitative element data were collected using a JEOL JXA-8530FPlus Electron Probe Microanalyzer (EPMA) (Fig. S2) in the Characterization Facility at the University of Minnesota. BSE images were collected with an accelerating voltage of 15kV and probe current of 15 nA. The qualitative element maps for Pb and Ca were collected using a probe current of 200 nA. Peaks were identified using Pb metal and Durango apatite. According to the factory documentation, the Pb detection limit for this microanalyzer is 30 ppm. Note the actual detection limits depend on analytical conditions.

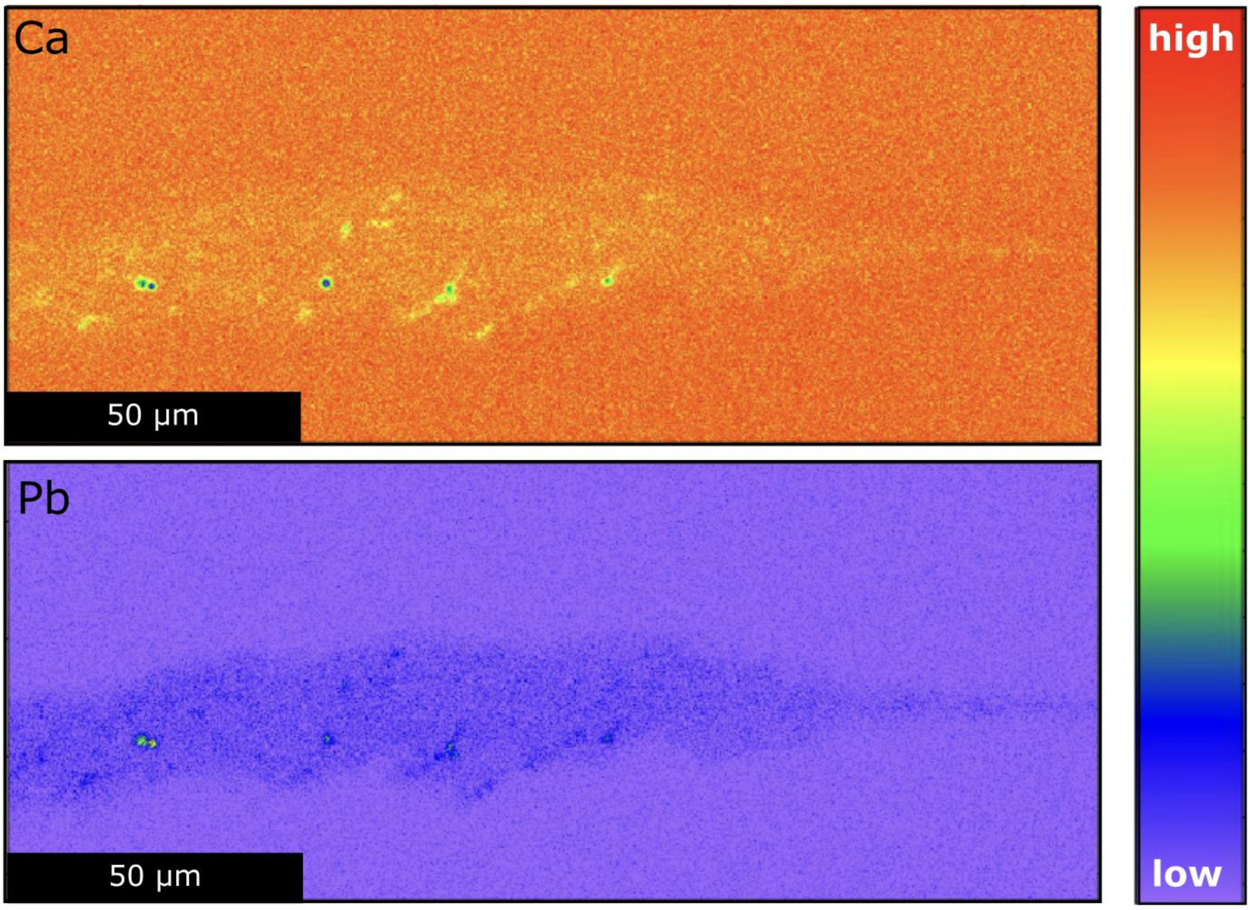

Figure S2. Qualitative EPMA data for relative concentrations of Pb and Ca.

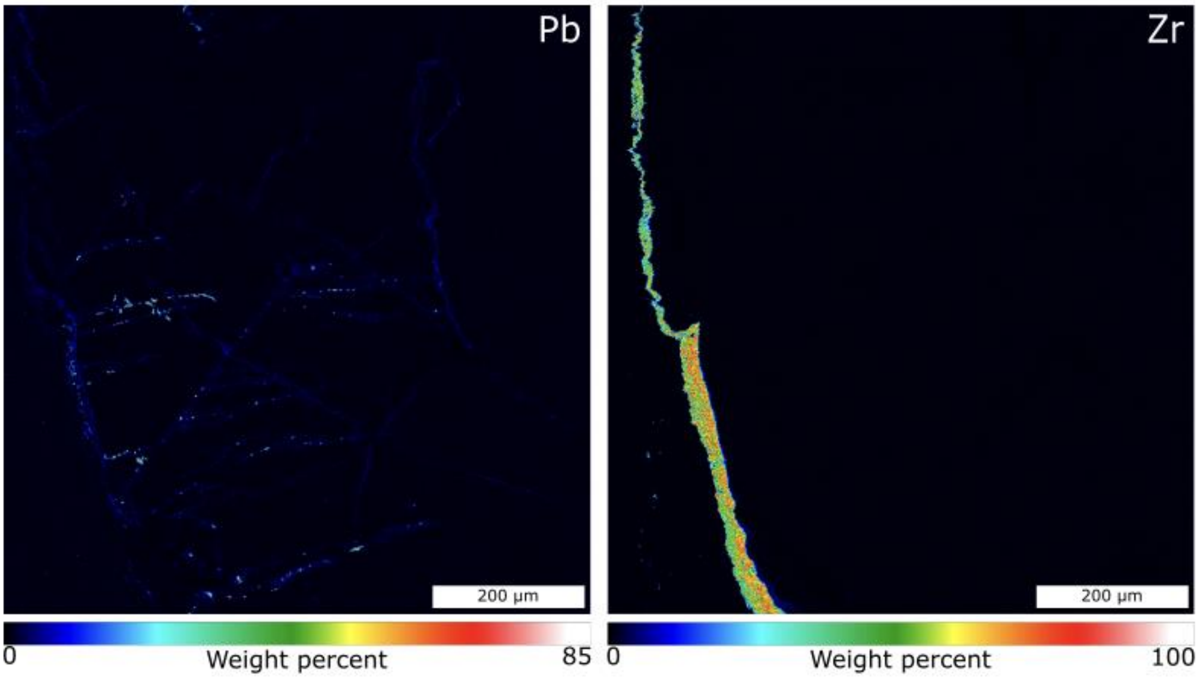

Figure S3. Quantitative sample-scale EPMA data for the dynamic diffusion experiment.

### *Results from null experiment*

The null experiment consisted of bringing a sample coated in $PbZrO_3$ to target conditions for 5 hours without deformation. This sample was sectioned, polished, and imaged with BSE as described above. The resulting BSE image (Fig. S4) exhibits no apparent heterogeneity, which is comparable to the static-diffusion experiment after torsion (Fig. 1C) and in contrast to the dynamic-diffusion experiment (Fig. 1D).

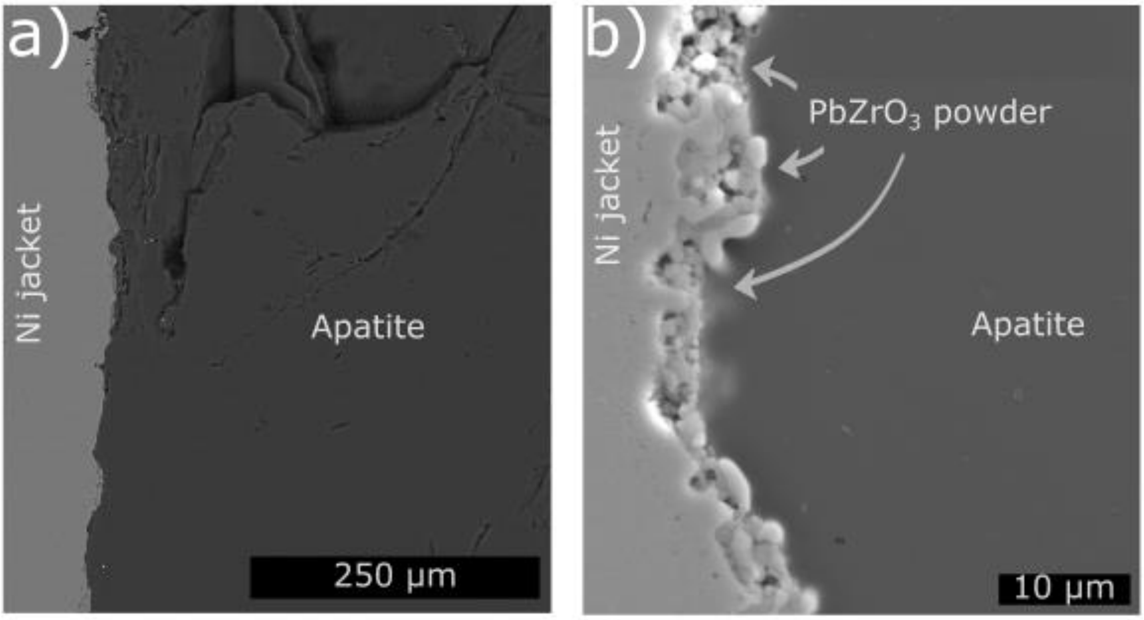

Figure S4A and B. BSE images of the null experiment.

## Supplementary References

Blavette, D., Cadel, E., Fraczkiewicz, A., and Menand, A., 1999, Three-dimensional atomic-scale imaging of impurity segregation to line defects: Science, v. 286, p. 2317–2319.

Cadel, E., Fraczkiewicz, A., and Blavette, D., 2003, Atomic Scale Investigation of Impurity Segregation to Crystal Defects: Annual review of materials research, v. 33, p. 215–231.

Fayon, A.K. and Hansen, L.N., 2018. Rheology of the rheologically insignificant mineral apatite. In *16th International Conference on Thermochronology*.

Frost, H.J. and Ashby, M.F., 1982. Deformation-mechanism maps: The plasticity and creep of metals and ceramics(Book). Oxford, Pergamon Press, 1982, 175 p.

Paterson, M.S., and Olgaard, D.L., 2000, Rock deformation tests to large shear strains in torsion: Journal of Structural Geology, v. 22, p. 1341–1358.